



Vibration and flexural performance of cross-laminated timber – glulam composite floors

Md Shahnewaz^a, Carla Dickof^b, Jianhui Zhou^{c,*}, Thomas Tannert^d

^a Specialist Engineer, Fast+Epp, Vancouver, Canada

^b Associate, Fast+Epp, Vancouver, Canada

^c Assistant Professor, School of Engineering, University of Northern British Columbia, Prince George, Canada

^d Professor, School of Engineering, University of Northern British Columbia, Prince George, Canada

ARTICLE INFO

Keywords:

Mass-timber construction
Cross-laminated timber
Floor vibration
Hybrid connections

ABSTRACT

This paper presents experimental research on composite cross-laminated timber (CLT) glulam floors. The composite action was achieved using three different types of connectors. The connector stiffness and strength were determined with small-scale shear tests. Quasi-static monotonic four-point bending and vibration tests were conducted on six full-scale (9.1 m long, 1.6 m wide) double T-beam floor segments consisting of 3-ply CLT panels and two glulam beams. The vibration test results indicated that the three connection types had negligible influence on the dynamic properties of the composite floor segments, while the allowable vibration controlled span of the composite panel was around 7.2 m with acceptable subjective evaluations. The load-deformation behaviour observed in the full-scale testing was linear up to failure which was brittle tension at mid-span in one of the glulam beams for all specimens. The ratio between experimental and expected bending stiffness was close to 1.0 for all three connector types demonstrating the adequacy of applying the gamma method to predict the performance of CLT-glulam composite floors. The findings from this research supported the design and construction of the floors for two new school buildings.

1. Introduction

1.1. Background

The structural use of timber in North America is no longer limited to labour intensive commodity products used in low-rise residential light-frame construction but the potential for larger and non-residential structures is increasingly being explored [1,2]. The resulting challenges, e.g. increased lateral forces and increased demand on floor serviceability, are being addressed by the introduction of innovative materials [3,4], connections [5,6], components [7] and composite systems [8], as well as changing legislation. e.g., the 2020 version of the National Building Code of Canada (NBCC) [9] allowed mass timber structures up to 12 storeys and the International Building Code (IBC) [10] included tall wood construction up to 18 storeys. Promising structural approaches involve cross-laminated timber (CLT), a mass timber product, consisting of sawn lumbers glued together in alternating directions; creating panels with high in-plane strength and stiffness

[11,12].

The School Board in Vancouver, British Columbia, Canada [13] commissioned two new buildings to replace existing elementary schools. The two-storey buildings include learning spaces with exposed CLT walls, floors, and roofs. Both projects include long-span floor or roof systems for which both deflection and vibration requirements fell outside the feasible range for even the thickest commercially available panels in North America (9-ply 315 mm thick panels). Therefore, a ribbed CLT-glulam composite was proposed, see Fig. 1. Natural Resources Canada, through the Green Construction Wood program [14], assisted with the project costs including a test program to support the innovative use of long-span timber-timber-composite (TTC) floors.

1.2. Timber floor serviceability requirements

The design of long-span floors is often governed by serviceability limit states, i.e. deflection and vibration [15,16]. Their dynamic properties are critical for determining their vibration response. NBCC [9] has

* Corresponding author.

E-mail addresses: mshahnewaz@fastepp.com (M. Shahnewaz), cdickof@fastepp.com (C. Dickof), Jianhui.Zhou@unbc.ca (J. Zhou), thomas.tannert@unbc.ca (T. Tannert).

<https://doi.org/10.1016/j.compstruct.2022.115682>

Received 26 April 2021; Received in revised form 25 January 2022; Accepted 24 April 2022

Available online 29 April 2022

0263-8223/© 2022 Elsevier Ltd. All rights reserved.

clearly defined deflection limits, but does not provide explicit vibration limits. The Canadian Standard for Engineering Design in Wood, CSA O86 [17], addresses the vibration performance of bare CLT panels supported on rigid supports (i.e. walls). The resulting required thickness, however, renders such CLT slabs inefficient for long-span applications.

Composite floor systems, joining members of similar or different materials, create a composite section with higher strength and stiffness than the simple addition of the separate elements, will improve all serviceability limit states. Such floors systems are not addressed in the standard. Various design guides and performance criteria are available for steel and concrete floors [18–20]. Guidance for mass timber floors, other than those included in CSA O86 [17], are addressed in the U.S. Mass Timber Floor Vibration Guide [21], this requires both laboratory and field verifications.

1.3. Timber-concrete systems

Timber-concrete composite (TCC) systems have been extensively studied in recent years using mechanical connectors [22,23], adhesive bonds [24] or a combination of both [25]. On TTC systems, fewer experimental, numerical, and analytical investigations have been reported. Experiments on multi-layered timber beams using wood dowels showed the possibility to achieve high composite action by increasing the number of dowels [26]. The possibility of strengthening and stiffening aged timber floors by means of composite actions using CLT top plates connected with screws installed at different angles showed that the 45° installation angle led to higher composite efficiency and stiffness [27]. A shear connection system for CLT-glulam composite floor systems made of double-sided punched metal plate fasteners has been claimed to be suited for automated production [28]. Investigations on CLT composite floors connected by inclined screws led to the proposal of a formula to estimate the effective width of the CLT panels [29]. Comparing fully and partially threaded screw connections showed that the former exhibited higher composite efficiency [30]. Numerical analyses on TTC systems with inclined screws achieved good agreement when compared to experimental results [31]. The long-term behaviour (1.5 years) of TTC floors assembled by connecting CLT slabs with solid wood joists under consideration of cambering and pre-stressing showed that the combined use of partially and double threaded screws is favorable [32]. Based on the commercial potential, product approval exists for TTC panels, e.g. [33].

1.4. Design of timber composite floors

The most popular and widely used timber composite system are TTC floors in which a timber beam or slab is connected to a concrete topping using shear connectors. TTC can overcome some of the inefficiencies associated with traditional light wood frame floors regarding strength, stiffness, structural fire rating, and vibration and thermal performance [8,22]. Numerous connectors from low to high stiffness are available as composite connectors: self-tapping screws, dowel-type shear keys, perforated steel plates, steel kerf plates, transverse notch connection etc. Where screws are used to provide the composite action between, either vertically installed partially threaded screws primarily acting in shear [5], or inclined fully threaded screws primarily acting in withdrawal [6]

are used. Hybrid joints in combination of mechanical connectors with adhesive provide robust and rigid composite systems [25,34].

TTC systems can be designed using EN 1995–1-1 [35], based on the gamma (γ) method originally developed by Möhler [36] where the composite action is quantified by estimating γ , ranging from 0.0 (no composite action) to 1.0 (full composite action or full rigid connection), see Equation (1). The γ -value, together with cross-sectional properties of timbers (herein CLT floor and glulam beams), allow estimating the effective bending stiffness $(EI)_{\text{eff}}$, of TTC composite system, see Equation (2).

$$\gamma = \frac{1}{1 + \frac{\pi^2 E_{\text{CLT}} A_{\text{CLT}} s}{kL^2}} \quad (1)$$

$$(EI)_{\text{eff}} = E_{\text{CLT}} I_{\text{CLT}} + \gamma E_{\text{CLT}} A_{\text{CLT}} a_{\text{CLT}}^2 + E_g I_g + \gamma E_g A_g a_g^2 \quad (2)$$

where, E_{CLT} , E_g , I_{CLT} , I_g and A_{CLT} , A_g are the moduli of elasticity, second moment of area, and cross-section area for CLT and glulam beam, L is the floor span, k is the slip modulus of the connector, s is the connector spacing, and a_{CLT} and a_g are the distances from the neutral axis of the composite section to the neutral axis of the CLT and glulam, respectively.

The maximum normal and bending stresses in CLT and glulam ($\sigma_{n, \text{CLT}}$, $\sigma_{m, \text{CLT}}$, $\sigma_{n, g}$, $\sigma_{m, g}$) elements can be calculated using Equations (3)–(6), the maximum shear stress in the glulam beams ($\tau_{g, \text{max}}$) can be calculated using Equation (7), and the fastener shear force in CLT-glulam interface (F_c) can be calculated using Equation (8).

$$\sigma_{n, \text{CLT}} = \frac{\gamma E_{\text{CLT}} a_{\text{CLT}} M_f}{(EI)_{\text{eff}}} \quad (3)$$

$$\sigma_{n, g} = \frac{\gamma E_g a_g M_f}{(EI)_{\text{eff}}} \quad (4)$$

$$\sigma_{m, \text{CLT}} = \frac{0.5 E_{\text{CLT}} h_{\text{CLT}} M_f}{(EI)_{\text{eff}}} \quad (5)$$

$$\sigma_{m, g} = \frac{0.5 E_g h_g M_f}{(EI)_{\text{eff}}} \quad (6)$$

$$\tau_{g, \text{max}} = \frac{0.5 E_g h_g^2 V_f}{(EI)_{\text{eff}}} \quad (7)$$

$$F_c = \frac{\gamma E_{\text{CLT}} a_{\text{CLT}} s V_f}{(EI)_{\text{eff}}} \quad (8)$$

where, h_{CLT} and h_g are the depths of CLT and glulam, respectively.

1.5. Objective

TTC systems consisting of CLT slabs and glulam ribs are a promising option for long-span floors. The deflection and vibration performances depend on the stiffness of the system, which in turn depends on composite action between slabs and ribs. The objectives of the research presented herein were to investigate the efficiency of various connectors, and the vibration and flexural performance of a double-T shaped

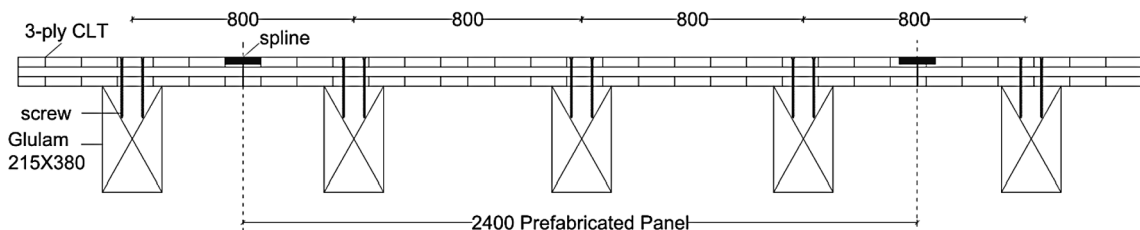


Fig. 1. Cross section of floor design for elementary schools.

TTC floor systems with these connectors. To achieve these goals, small-scale shear and full-scale bending and vibration tests were conducted. The performance of the connectors was evaluated in terms of capacity, stiffness, and ductility, whereas the performance of the TTC floors was evaluated in terms of frequency, acceleration, load carrying capacity, deflections, stiffness, and slips at timber-timber interfaces.

2. Experimental investigation

2.1. Materials and specimen description

The CLT panels and glulam beams were fabricated by Structurlam in accordance with ANSI PRG 320 [37] and CSA O122 [38]. A summary of the material properties is provided in Table 1, with the specified bending strength values based on CSA O86 tabulated values [17].

A total of six composite (double T-beam cross-section) specimens composed of a single CLT panel and two beams, as shown in Fig. 2, were assembled and subsequently tested in the Wood Innovation Research Lab at the University of Northern British Columbia.

Three connection types were investigated with two specimens each:

- Type A: 10Ø × 200 mm ASSY SK partially threaded washer head self-tapping screws with longitudinal spacing of 75 mm on centre installed at 90°, see Fig. 3a.
- Type B: 8Ø × 300 mm ASSY VG fully threaded self-tapping screws with longitudinal spacing of 150 mm on centre installed at 45°, see Fig. 3b.
- Type C: 10Ø × 200 mm ASSY SK partially threaded washer head self-tapping screws with longitudinal spacing of 300 mm on centre installed at 90°, see Fig. 3c, in combination with an adhesive bond provided by a one-component polyurethane adhesive (LePage Premium PL). The specific gravity and viscosity of the adhesive are 1.71 and 1,200,000 cps, respectively [39]. For typical wood surface application, the open time is 15–20 min at 25 °C and 50% relative humidity and the cure time is 24–48 h. The reported shear strengths as per ASTM D 3498 [40] are 4.9 MPa and 8.8 MPa for dry and wet lumber bonding, respectively, on Douglas Fir.

Both mechanically fastened connections (types A and B) were designed to be sufficiently strong to fail the system in glulam tension failure.

The expected factored standard-term duration shear force resistances of Type A and Type B connectors were 2.4 kN and 5.7 kN per screw, respectively, calculated using the properties provided in the product approval evaluation report [41] and design catalogue [42], respectively, and the design provisions for lag screws according to CSA O86 [17] and the product approval evaluation report [41], respectively. These expected resistances correspond to factored 5th percentile values. The expected serviceability limit state stiffness, K_{ser} , of Type A and Type B connectors was 4.3 kN/mm and 37 kN/mm per screw, respectively, based on EN 1995–1-1 [35], see Equation (9), and the European Technical Approval [43], see Equation (10).

$$K_{ser} = \rho_m^{1.5} d / 23 \quad (9)$$

Table 1
Material description.

	CLT	Glulam
Species	S-P-F	Douglas-Fir
Grade	105 V, V2M1.1	24f-E
Cross section	1,162 mm × 105 mm	215 mm × 380 mm
Length	9,144 mm	8,944 mm
Density	441 kg/m ³	545 kg/m ³
Moisture content	11%	12%
Bending strength	11.8 MPa	30.6 MPa

$$K_{ser} = 780 d^{0.2} l_{ef}^{0.4} \text{ [N/mm]} \quad (10)$$

where, ρ_m is the product of the square roots of the density of the two jointed wood materials, d is the shank diameter of the screw, and l_{ef} is the penetration length of the screw.

The glued connection (type C) had a reduced number of screws with the intent to achieve full composite action through the glued interface. As discussed subsequently, each connection type provided a different level of composite action, resulting in different stiffnesses and slip between the panel and the beam.

Fig. 4a and 4b show the installation of screws inclined at 45° and 90° for the connector types B and A, respectively. Fig. 4c and 4d show the adhesive applied to the glulam beams. Four 825 ml cartridges were applied to each glulam beam, illustrated in Fig. 4c, creating a layer of approximately 1.8 mm thickness. The CLT panels were installed within the glue's open time of 30 min. After the screw installation, some excess glue was pushed out on the sides, see Fig. 4d. No post-test bond-quality control was conducted. Therefore, small un-bonded areas may have been present and remained undetected, which was not explicitly considered. However, any potential variation in strength would have had negligible impact on the system overall because small variations in strength did not appear to impact the strength of the system.

2.2. Small-scale shear tests

The three connection types were tested to determine their shear strength and stiffness to provide a basis to verify the composite design. Four replicates were tested under monotonic loading for each connection type. These specimens were assembled using material sampled after the full-scale floor bending tests. The CLT panels were 275 mm wide and 600 mm long and glulam beams were 215 mm wide and 600 mm long, see Fig. 5.

The test set-up consisted of a compression load frame, as shown in Fig. 6. Test specimens were rotated by 13.5° as suggested in EN-408 [44]. The loads were applied according to the EN-26891 [45] protocol at a displacement-controlled rate of 5 mm/min for the specimens with connector Type A and 1 mm/min for the specimens with connector Types B and C. Specimens were loaded to 40% of the estimated capacity, then unloaded to 10% of estimated capacity, and finally loaded to failure, defined as the point when load dropped to 80% of the maximum.

The actuator load and the relative vertical displacements between CLT and glulam were measured using two calibrated LVDTs, one on each side of the specimen, attached at mid-height. The reported displacements are the averages between the two measurements. The connector performance was analyzed at the maximum load F_{max} , displacement at maximum load d_{Fmax} , serviceability (elastic) stiffness K_{ser} computed for the range between 10% and 40% of F_{max} , ultimate stiffness K_u computed for the range between 0% and 60% of F_{max} , as well as ductility μ . In addition, the yield load F_y and the displacement at yield d_y were determined based on equivalent energy elastic plastic (EEEP) curves [46], see Fig. 6c. The failure at ultimate load F_u is defined as of $0.8F_{max}$ from the post-peak region of the load–displacement curves; the ultimate displacement d_u corresponded to F_u . Ductility was defined as the ratio of ultimate to yield displacement (d_u/d_y).

2.3. Modal tests of composite floor specimens

The floors' dynamic properties were investigated by modal tests and analysis. After assembling and measure the mass of each specimen, impact hammer tests and modal analysis, as illustrated in Fig. 7a, were conducted to determine the natural frequencies, corresponding mode shapes and damping ratios. The support boundary conditions were realized with rollers as shown in Fig. 7b and 7c. The floor specimens were tested via the roving hammer method for modal analysis with natural frequencies, mode shapes and damping ratios under 50 Hz

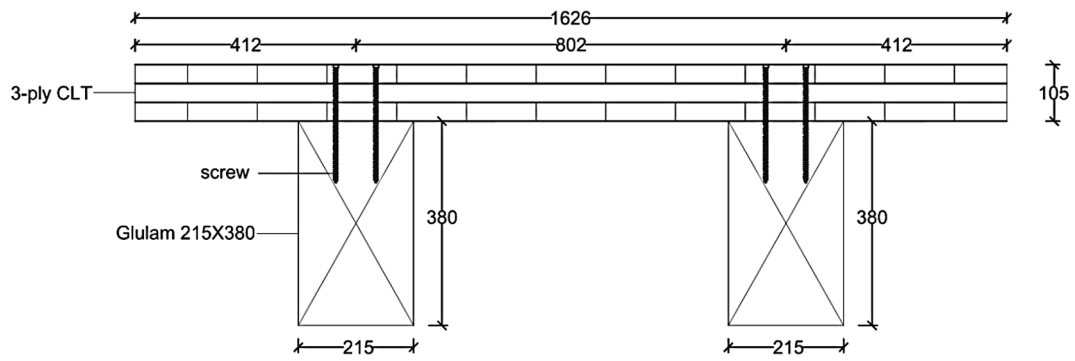


Fig. 2. Cross section of test specimens [measurements in mm].

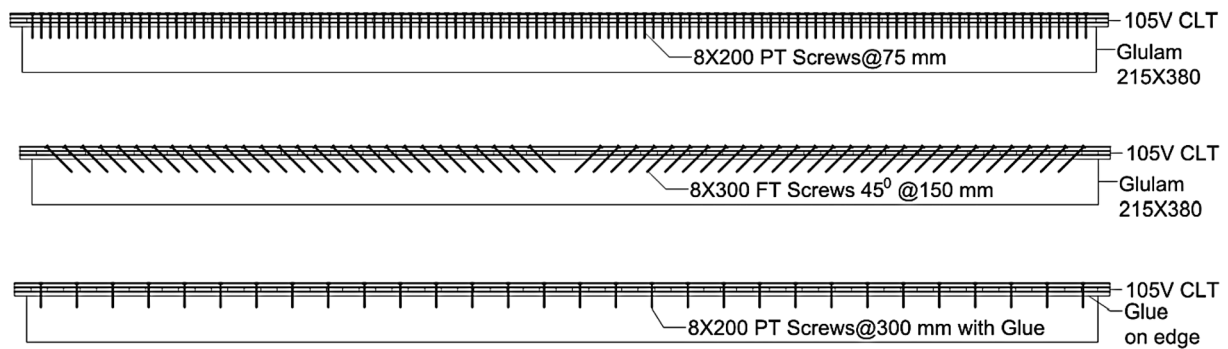


Fig. 3. Schematic of test specimens: (a) Type A - screws at 90°; (b) Type B - screws at 45°; (c) Type C - screws at 90° with glue.

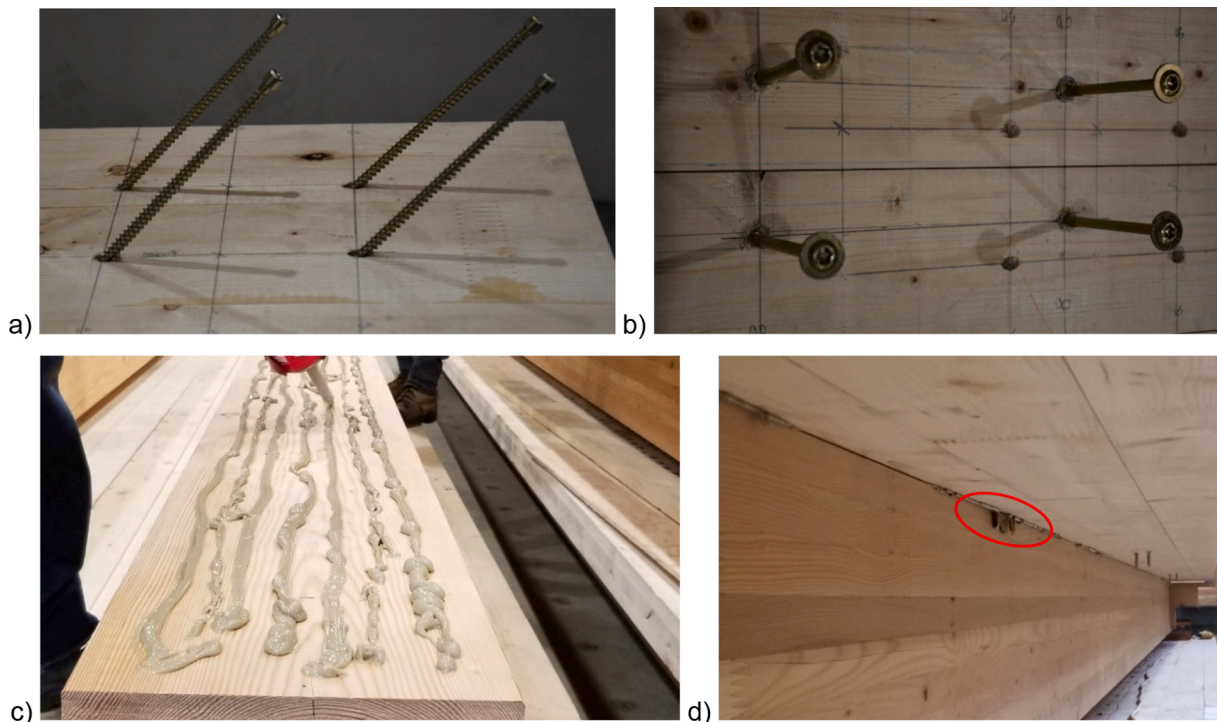


Fig. 4. Specimen fabrication: Screws installation (a) at 45° and (b) 90°; application of glue to glulam beam (c) and fully glued cross-section (d).

obtained for each specimen.

To investigate the influence of boundary conditions on the dynamic performance, floor specimen DT-4 was also tested with two end support conditions: 1) DT-4-0 with the glulam beam supports at the two ends; and 2) DT-4-1 with the CLT end walls with partially threaded self-

tapping screws at a spacing of 250 mm as shown in Fig. 7d. Subsequently, the fundamental natural frequency of the simply supported glulam beam can be estimated based on measured density and modulus of elasticity, see Equation (10):

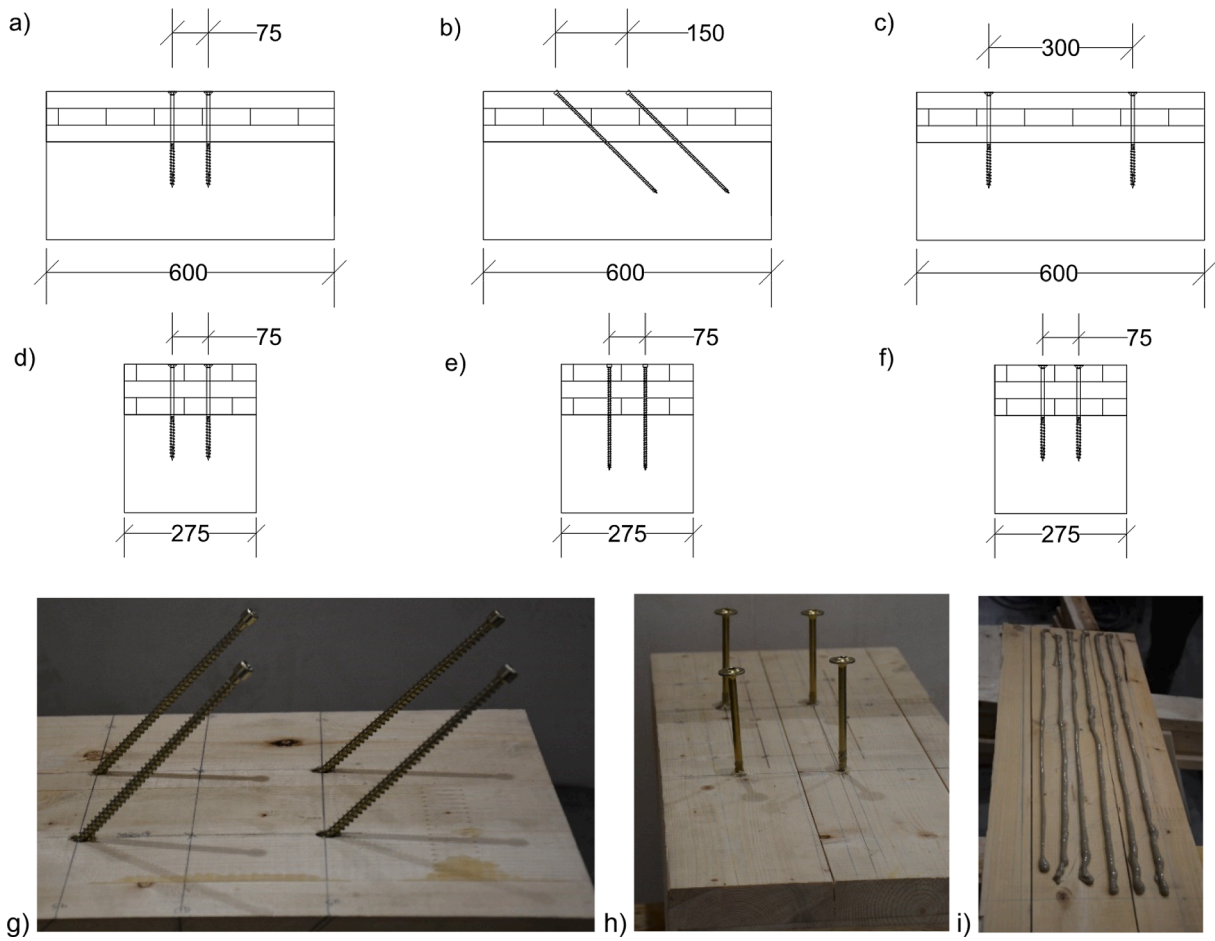


Fig. 5. Small-scale specimen layout: longitudinal cross-section of Type A (a), Type B (b), Type C (c); transverse cross-section of Type A (d), Type B (e), Type C (f); photos of Type A (g) Type B (h), Type C (i).

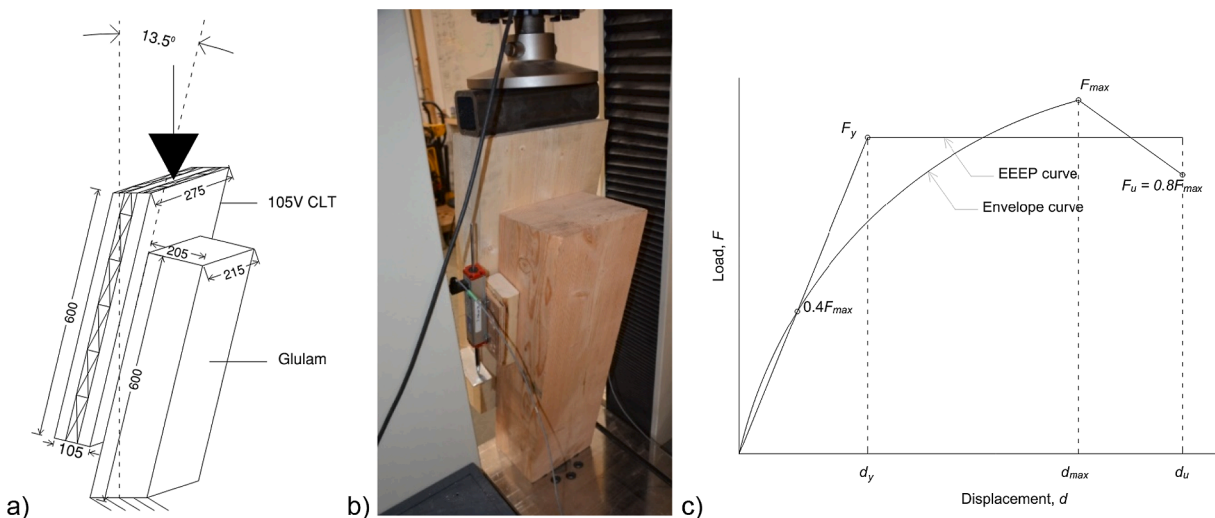


Fig. 6. Small-scale connector shear tests: (a) schematic [dimensions are in mm], (b) photo of test specimen, (c) EEEP curve for result analysis.

$$f = \frac{\pi}{2l^2} \sqrt{\frac{EI}{\rho A}} \quad (10)$$

2.4. Composite floor vibration response tests

Vibration tests were conducted on each floor according to ISO 10137

[47] and ISO 18324 [48] to determine the floors' natural frequencies and acceleration levels under normal walking by one person. The tests were performed by a 75 kg evaluator floor end to end with a step frequency of approximately 2 Hz, see Fig. 8.

The acceleration responses were measured at certain locations on the floor surface as shown in Fig. 9a. Four accelerometers were mounted on

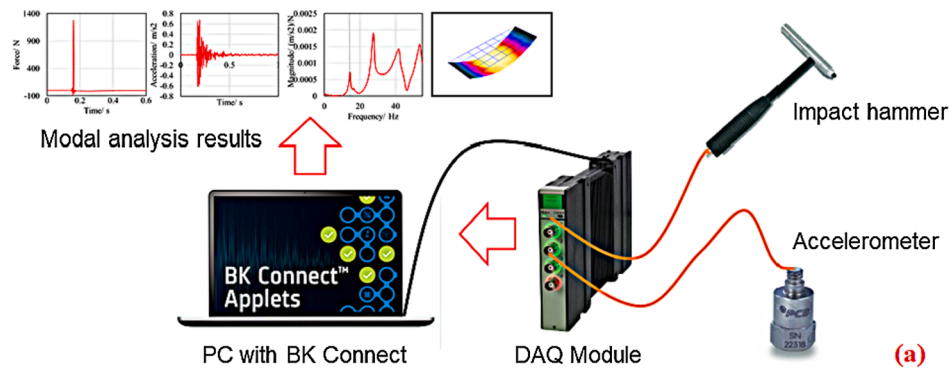


Fig. 7. (a) Impact hammer modal test and analysis, (b) T-beam specimen under test; (c) roller end supports, (d) wall/beam support.



Fig. 8. Walking tests on the T-beam floors (a); specimen with intermediate supports (b).

the floor surface as shown in Fig. 9a. The time domain acceleration data were post processed according to the flowchart as shown in Fig. 9b based on ISO 2631–2 [49]. Subjective evaluations, per ISO 21136 [50], were conducted for the acceptance level of the composite floors, categorizing the floors into levels 1 to 5, i.e. 1 = definitely unacceptable, 2 = unacceptable; 3 = marginal, 4 = acceptable, 5 = definitely acceptable. A survey with 10 evaluators was conducted on each floor. The evaluator first walked on the floor between two ends, and then stood stationary at the center of the floor while a 75 kg walker walked between the two ends. Each evaluator completed a questionnaire provided in ISO 21136 [50]; all evaluator ratings for each floor specimen were averaged and reported as final rating.

Additionally, double-span tests were completed with specimen DT-4 by adding mid-span supports made of glulam blocks under the glulam

beams as shown Fig. 8b, which added restraints in the vertical direction; the double-span floor tests included four span ratios: 3) DT-4–2 ratio of 2:1; 4) DT-4–3 ratio of 3:1; 4) DT-4–4 ratio of 4:1; and 5) DT-4–4 ratio of 7:1. The intent was to determine an approximate span that could achieve a subjective rating of 3 or higher, defined as when the evaluator did not feel much vibration as a walker and could accept the vibration level as a standing observer. Similarly, the accelerometers were mounted on the center point and the midpoint on the free edge for each span.

2.5. Full-scale bending tests

The destructive 4-point bending tests included a set-up with two 500 kN actuators, positioned as shown in Fig. 10. A total of six string pots, labelled S1 to S6 and eight linear variable differential transducers

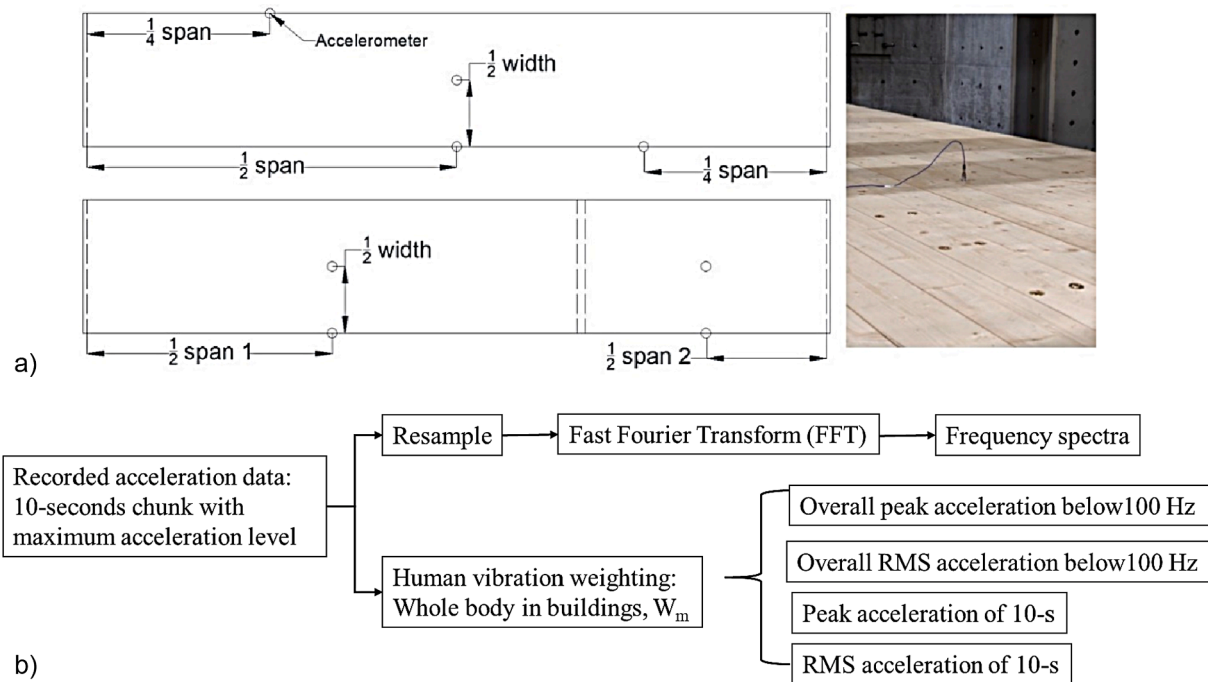


Fig. 9. Acceleration measurement points (a); Post-processing flowchart of acceleration data (b).

(LVDTs) labelled L7 to L14 were installed to measure the overall vertical deflections and the relative horizontal displacements between CLT and Glulam respectively, see Fig. 10.

The floors were subjected to quasi-static monotonic loading at a constant rate of 10 mm/min until floor failure, where failure was defined as a drop in the applied load by >20%. The loading protocol involved performing an initial pre-load cycle to 40% of the anticipated ultimate load-carrying capacity. The maximum force, F_{max} , and its corresponding mid-span deflection, d_{Fmax} , were determined based on the actuator load and the average of string pots S3 and S4. In addition, the slips (relative horizontal displacement between glulam and CLT components) at locations of floor edges, $S_{e,Fmax}$ and at distance of a ($0.3L$ or $0.7L$, where L is span length), $S_{a,Fmax}$ were recorded using the LVDTs #7–8, #13–14 and LVDTs #9–12, respectively, as shown in Fig. 10a. The load increase from 10 to 40% of maximum force (F_{max}), ΔF_{10-40} , and the corresponding increase in deflection, Δd_{F10-40} , allowed calculating the apparent static bending stiffness, EI_{app} , using Equation (11):

$$EI_{app} = \frac{\Delta F}{48\Delta d} \cdot (3L^2a - 4a^3) \quad (11)$$

where L is the span and a is the distance from the support to the point load, herein 3,048 mm.

3. Results and discussion

3.1. Small-scale shear connector tests

The results of the small-scale tests are presented in Table 2. Type A connectors reached the lowest load-carrying capacity, yield and ultimate strengths ($F_{max} = 80$ kN; $F_y = 65$ kN; $F_u = 64$ kN). These metrics for Type B connectors were on average 30% higher. When compared to the un-factored design values ($F_d, Type A = 18.7$ kN; $F_d, Type B = 41.5$ kN) for short-term loading as per CSA O86 [17] and the ASSY CCMC Evaluation Report [41] respectively, F_{max} is about four and three times higher, respectively. The CSA O86 [17] lateral resistance equations for lag screws are based on research with large diameter screws require significant reduction factors due to group factors, connection slips, and pre-drilling requirements, low reliability, and limited rope effect. The self-

tapping screws used herein do not require pre-drilling, and have significant withdrawal strength increasing the impact of rope effect; therefore, the CSA O86 should be expected to be overly conservative. Recent experimental findings presented ratios between experimental and design values up to 11.

Type C connectors reached values that were more than three times higher than Type A connectors ($F_{max} = 256$ kN; $F_y = 236$ kN; $F_u = 205$ kN). However, it has to be reminded that both mechanical connections could also be designed for higher strength by increasing the number of screws per unit length. Variability between replicates within the test series was small with around 5% for all metrics, other than the yield strength of the glued connectors with 9%.

Type A connectors reached the largest deformations at maximum load, at yield and at ultimate load ($d_{Fmax} = 67$ mm; $d_y = 11$ mm; $d_u = 101$ mm). The deformations of Type B connectors were significantly lower ($d_{Fmax} = 3$ mm; $d_y = 2$ mm; $d_u = 6$ mm), showing the limited deformation capacity of screws installed at 45° and acting primarily in withdrawal. Type C connectors exhibited very small deformations of approximately 0.1 mm at yield and 0.3 mm at ultimate loads. Consequently, the stiffness observed for Type A connectors was low ($K_{ser} = 6$ kN/mm; $K_u = 2$ kN/mm) while stiffness of Type B connectors was high ($K_{ser} = 43$ kN/mm; $K_u = 47$ kN/mm). For both connectors, the experimental results were in good agreement with the expected values. Type C connectors achieved very high stiffness ($K_{ser} > 2,000$ kN/mm) and can be deemed rigid for practical purposes. The average ductility, calculated from the EEEP curves, for connector types A and B were 9.2 and 2.7, respectively. Since deformations were very small, no ductility was computed for type C connectors. Variability of deformation and stiffness metrics for type A and B connectors was between 9% and 22%; due to the very small values, variation between the test specimens with glued connectors was larger, exceeding 50%.

The load–displacement curves of all small-scale specimens are illustrated in Fig. 11 where d is the average of the two measurements. Type A connectors with screws installed at 90° had smooth curves until failure loads with relatively small initial stiff part up to 1.5 mm. Type B connectors with screws installed at 45° exhibited clear bi-linear curves with initial high stiffness until they reached to the screw’s withdrawal capacity. Type C with glue was very stiff and exhibited very small

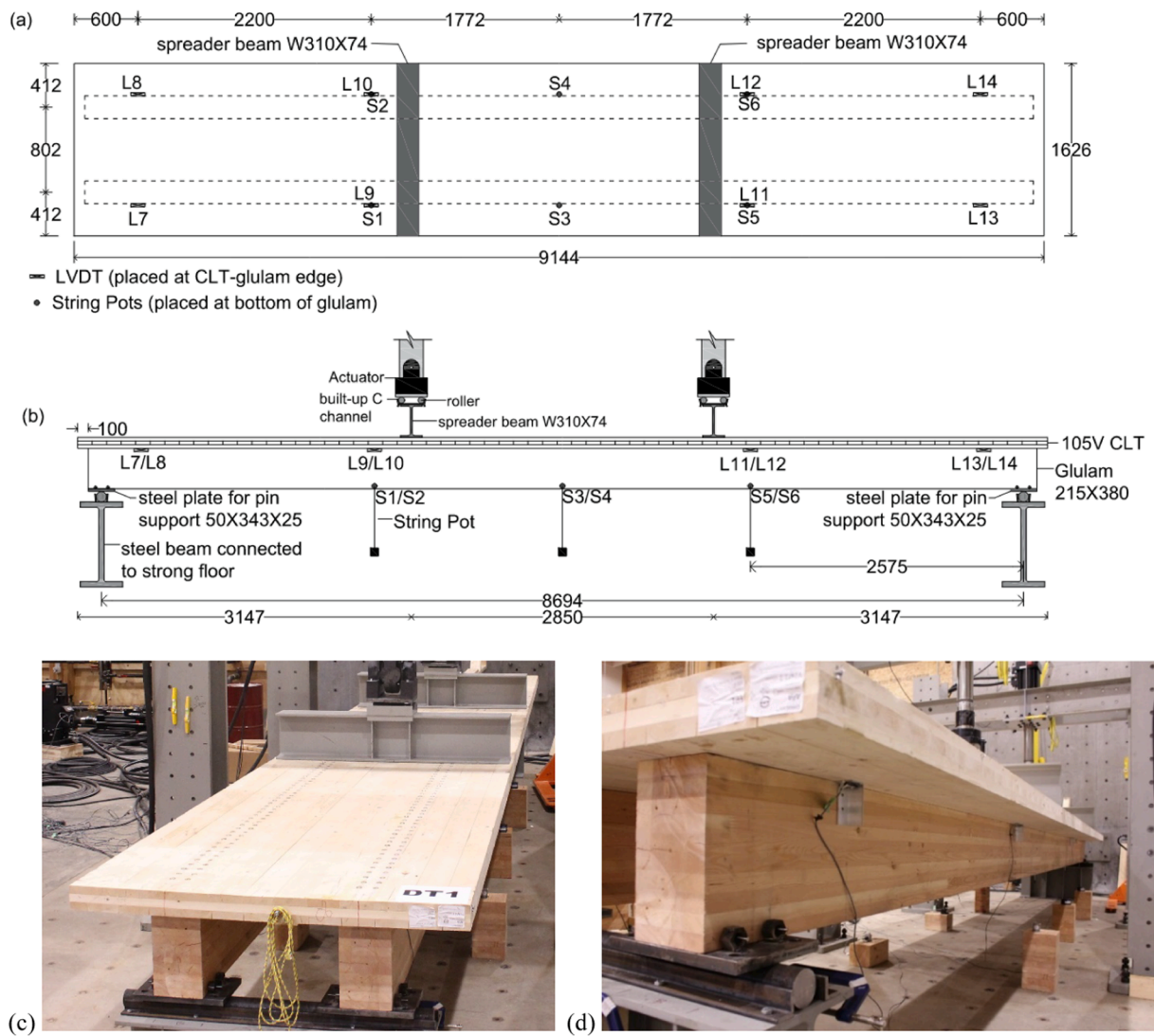


Fig. 10. Schematics (a) and (b) and photos (c) and (d) of 4-point bending setup and location of measurement devices.

Table 2
Results of small-scale shear tests.

ID	Connector	F _{max} [kN]	d _{Fmax} [mm]	K _{ser} [kN/mm]	K _u [kN/mm]	F _y [kN]	d _y [mm]	F _u [kN]	d _u [mm]	D [-]
A1	10Ø×200 mm PT@90°	77	56	7.7	2.9	63	8.3	61	97	11.8
A2		81	70	5.2	2.2	67	13.0	65	98	7.5
A3		78	67	5.2	2.1	63	12.2	62	86	7.1
A4		84	76	5.6	1.7	67	12.1	67	124	10.3
Mean		80	67	5.9	2.2	65	11.4	64	101	9.2
CoV		4%	13%	20%	22%	4%	18%	4%	16%	24%
B1	8Ø×300 mm FT@45°	102	3.0	40	44	95	2.4	81	6.1	2.6
B2		107	2.9	50	53	98	2.0	85	6.3	3.2
B3		106	3.2	40	45	103	2.6	85	6.1	2.4
B4		98	2.8	43	46	91	2.1	78	5.2	2.4
Mean		103	3.0	43	47	96	2.3	82	5.9	2.7
CoV		4%	5%	11%	9%	5%	12%	4%	9%	15%
C1	10Ø×200 mm PT @90° with glue	257	0.2	>2,000	>2,000	221	0.1	206	0.2	
C2		244	0.3	>2,000	>2,000	221	0.1	195	0.5	
C3		268	0.4	>2,000	>2,000	266	0.2	214	0.5	
C4		265	*	*	*	*	*	*	*	
Mean		256	0.3	>2,000	>2,000	236	0.1	205	0.4	
CoV		5%	39%	>50%	>50%	9%	>50%	5%	49%	

*No displacement recordings available for specimen C4.

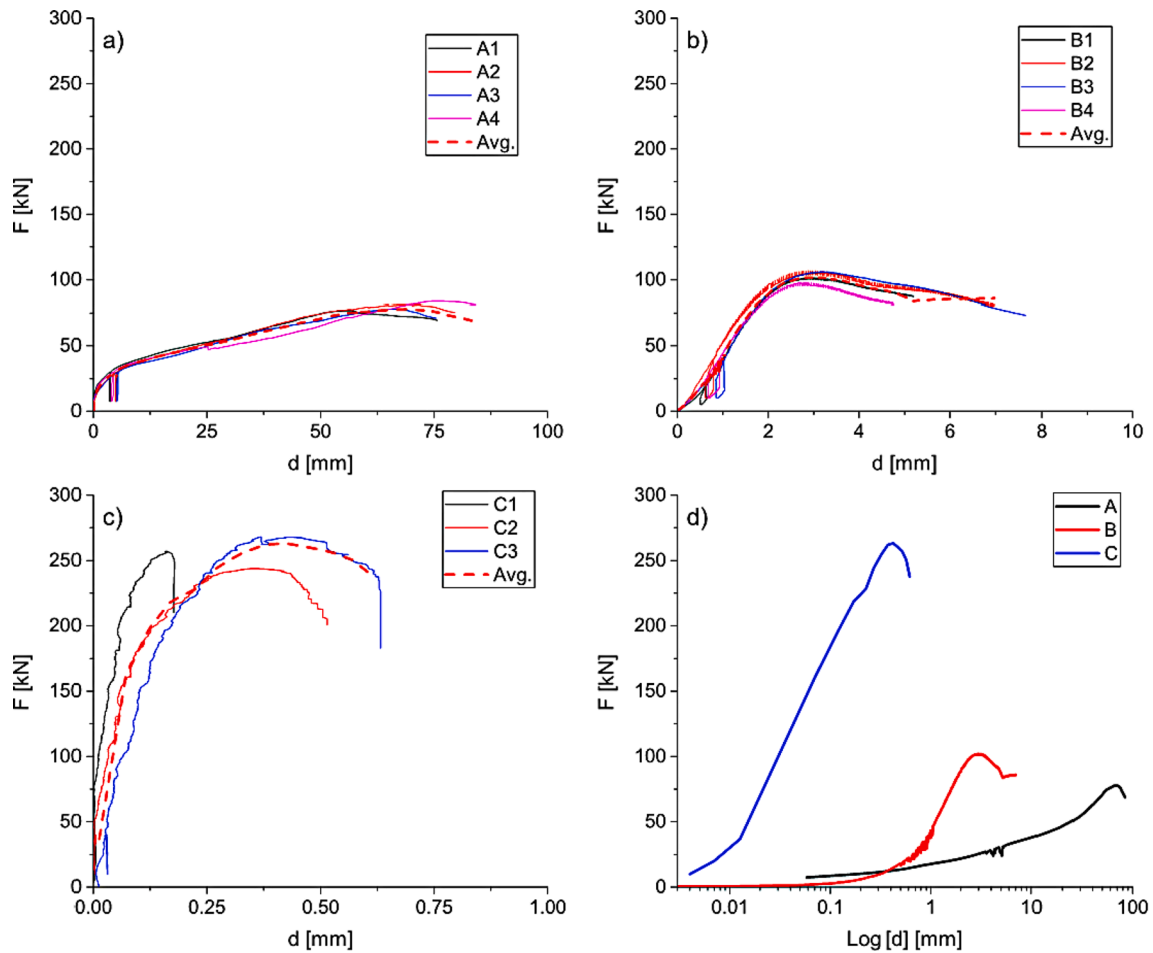


Fig. 11. Small-scale specimen load–displacement curves: (a) Type A, (b) Type B, (c) Type C, (d) average of Type A, B, and C curves in log scale.

displacements until failure, with failure being brittle in nature.

3.2. Dynamic properties of composite floor specimens

The natural frequencies of each composite floor are listed in Table 3 with corresponding mode shapes illustrated in Fig. 12. The fundamental natural frequencies of all specimens were between 12 and 13 Hz, with no significant differences among the three groups; the damping ratio of the fundamental natural frequency mode is 2.4% on average. It is thought that the fundamental natural frequency of the composite floor specimens is mainly governed by the glulam beams. The fundamental natural frequency of the simply supported glulam beam was approximately 11 Hz using Equation (4). Therefore, the connection had little influence on the dynamic properties of the composite floor specimens. The mode shape is expressed using mode indices (m, n), where, m and n are the number of node lines including the simply supported sides in minor and major

Table 3
Natural frequencies of simply supported floor specimens by modal tests and analysis.

Specimen #	Mass (kg)	Span (m)	Natural frequencies (Hz)					
			$f_{(2,0)}$	$f_{(2,1)}$	$f_{(1,1)}$	$f_{(2,2)}$	$f_{(3,0)}$	$f_{(3,1)}$
DT-1	1,548	8.84	12.3	15.8	25.0	36.5	37.0	43.0
DT-2	1,530	8.84	12.5	14.9	29.8	39.6	-*	43.1
DT-3	1,574	8.84	12.9	15.8	22.1	36.9	39.4	41.7
DT-4	1,523	8.84	12.8	15.9	31.5	38.8	37.9	42.3
DT-5	1,554	8.84	12.2	14.5	29.6	34.8	35.6	36.8
DT-6	1,544	8.84	12.9	14.9	23.6	34.3	36.8	39.1

*No data available.

strength directions, respectively. Due to the unrestrained edges of CLT flange panels, there are modes like mode (1,1) found for composite floor specimens, which are normally found for a plate with four free edges. The higher frequency modes such as the torsional mode and bending mode in the minor strength direction are governed by the CLT panel.

3.3. Vibration serviceability performance of composite floor specimens

The vibration performance indicators were determined from walking tests. Subjective evaluations of each single-span floor segment were rated as unacceptable under the test support condition. The fundamental frequencies under single person walking excitations were similar to those measured by impact hammer tests with transient response, see Fig. 13 and Table 4. Only the DT-4 results are presented as all the single-span specimens showed similar response and subjective evaluations. The acceleration time history and frequency spectra responses are shown in Fig. 13 for DT-4 with the different support configurations. The acceleration response was taken from the accelerometer with the largest peak acceleration values; in most cases the acceleration response was highest at the geometric center of the longer span, and the fundamental frequency mode dominated the response. Where the acceleration response at the edge was higher, then higher modes such as modes (2,1) and (1,1) are observed as the dominant mode in the frequency response spectra.

The variation in end constrains (DT-4-0 and DT-4-1) did not appear to affect the fundamental frequency and/or the response of the system. The results of floors with intermediate supports reducing the span shows reduction in vibration response and increase in fundamental frequency; a span that achieves the performance target of a subjective evaluation of 3 appears to be approximately 7.2 m based on the single floor segment. It

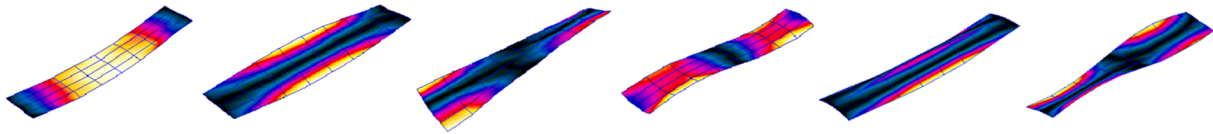


Fig. 12. Experimental mode shapes of the T-beam floor specimens under 50 Hz, mode (2,0), mode (2,1), mode (1,1), mode (3,0), mode (2,2), mode (3,1).

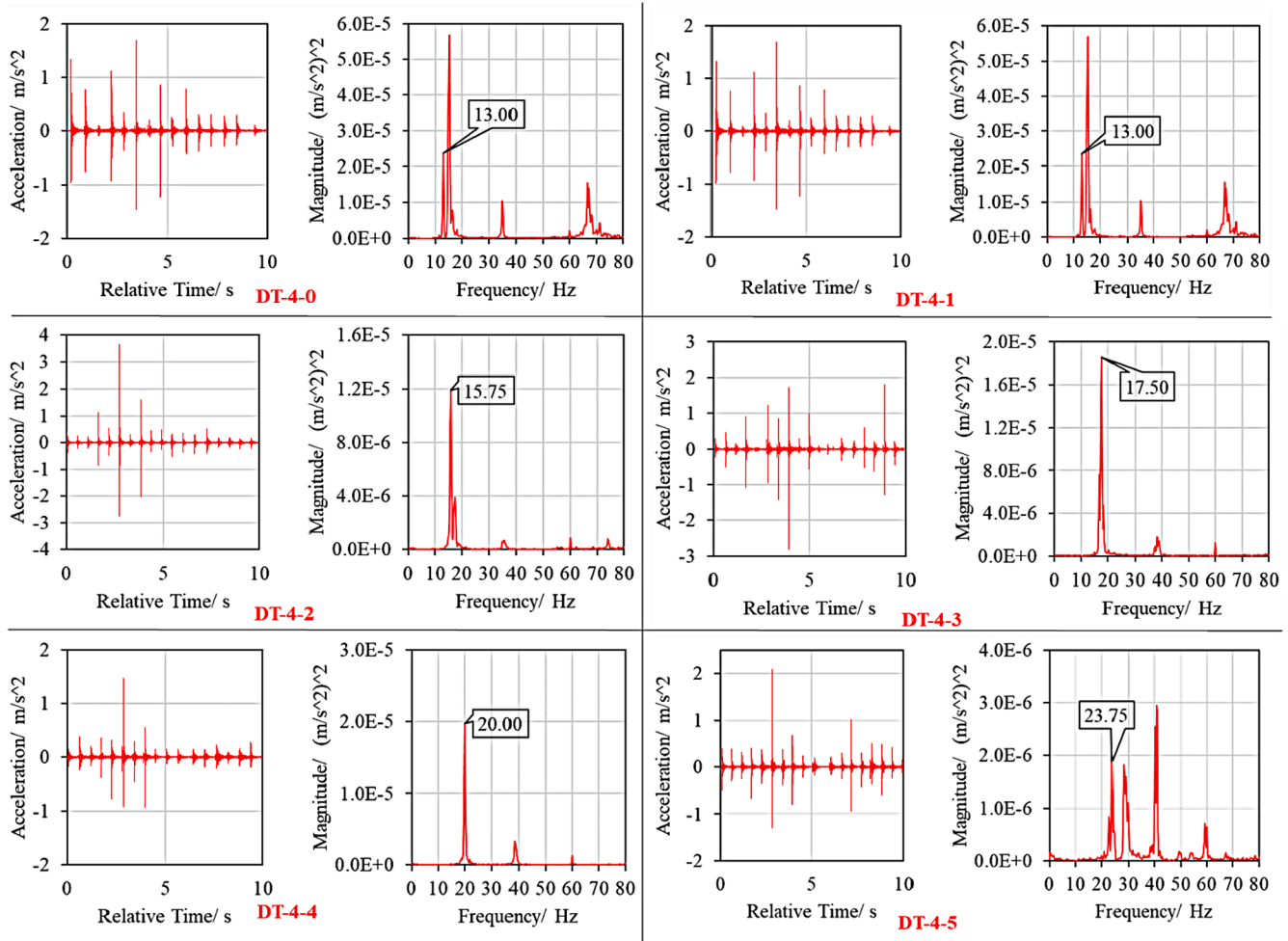


Fig. 13. Time-domain acceleration signal and frequency spectrum for DT-4 with intermediate supports: DT-4-0 (span 8.8 m with only glulam beam supports), DT-4-1 (span 8.8 m with additional wall supports), DT-4-2 (span 7.9 m), DT-4-3 (span 7.2 m), DT-4-4 (span 6.7 m), and DT-4-5 (span 5.9 m).

Table 4
Vibration performance indicators of composite floor specimen DT-4.

Test	Span (m)	f_1 (Hz)	Weighted acceleration (m/s^2)				Rating
			$a_{w,peak,100Hz}$	$a_{w,rms,100Hz}$	$a_{w,peak,10s}$	$a_{w,rms,10s}$	
DT-4-0	8.84	13.0	0.178	0.020	1.700	0.043	1
DT-4-1	8.84	13.0	0.149	0.020	1.700	0.044	1
DT-4-2	7.90	15.8	0.127	0.017	3.650	0.052	1
DT-4-3	7.15	17.5	0.228	0.022	1.810	0.049	3
DT-4-4	6.65	20.0	0.126	0.017	1.480	0.031	4
DT-4-5	5.90	23.8	0.104	0.017	2.100	0.038	5

should be noted that the field floor will have panel-to-panel connections between segments and a 50-mm thick concrete topping. Moreover, the measured vibration acceleration levels seem to have a low correlation with subjective ratings, though the same walker was used during all the tests.

The peak acceleration level of the 10-s time duration, $a_{w,peak,10s}$,

seemed to be the least reliable indicator compared with the other three, $a_{w,rms,100Hz}$, $a_{w,peak,100Hz}$ and $a_{w,rms,10s}$. The peak acceleration shown in Fig. 13 can be greatly affected by the walker, walking path, boundary conditions and any random perturbation from a single footfall impulse excitation. The root-mean-square acceleration levels are about the same magnitude with the vibration criteria recommended in ISO 10137 [47]

based on the building vibration z-axis base curve for acceleration. However, the measured values do not align well with subjective evaluations. Further investigations are required if experimental acceleration levels are used as a floor vibration performance indicator.

3.4. Full-scale bending tests

The load-deformation curves from the full-scale bending tests are illustrated in Fig. 14 with the deformations being the average measurements recorded on both glulam beams. The behaviour of the composite floors was linear up to failure. No stiffness degradation was observed as after the pre-loading to approximately 40% of expected capacity.

The results from the full-scale bending tests are summarized in Table 5. Composite floors with Type A connectors reached the lowest average load-carrying capacity ($F_{\max} = 371$ kN) at an average displacement of $d_{F_{\max}} = 103$ mm. Both specimens followed the same load-deformation; however, DT1 failed at a significant lower load and deformation compared to DT2. This result can be explained by the large variability of brittle strength values of timber. The average capacity of floors with Type B connectors was 438 kN, 18% higher compared to Type A floors, similar to the floors with Type C connectors. The deformation at failure of floors with Type C connectors was the lowest due to stiffest composite connectors. Both specimens with connectors Type B and C specimens also followed similar load-deformation pattern until failure, and the variation in failure loads between two replicates was approx. 15%. Significant differences were observed between the apparent bending stiffnesses as a function of connector type. As observed in small-scale tests, the application of glue in the composite floors with Type C connectors created a very stiff system. The average apparent bending stiffness, EI_{app} of Type C floors was 71,900 kNm², whereas Type A and Type B floors reached only 55,500 kNm² and 60,200 kNm², respectively.

Table 5 also includes the average slips at failure at edges $S_{e,F_{\max}}$, and at location a (0.3L) $S_{a,F_{\max}}$ at eight different locations along the interface of CLT-glulam. In Fig. 15, the average slips are illustrated. The slips in floors Type A were higher compared to floors with Type B connectors (more than twice as high), and floors with Type C connectors had negligible slips (only 0.2 mm at the edges which was 4% of the slips observed in Type A). The variations of average slips observed in both Type A and B floors were quite high, i.e., CoV of 42% and 41%, respectively compared to Type C with CoV of only 3%.

The photos in Fig. 16 show exemplarily the failure of selected

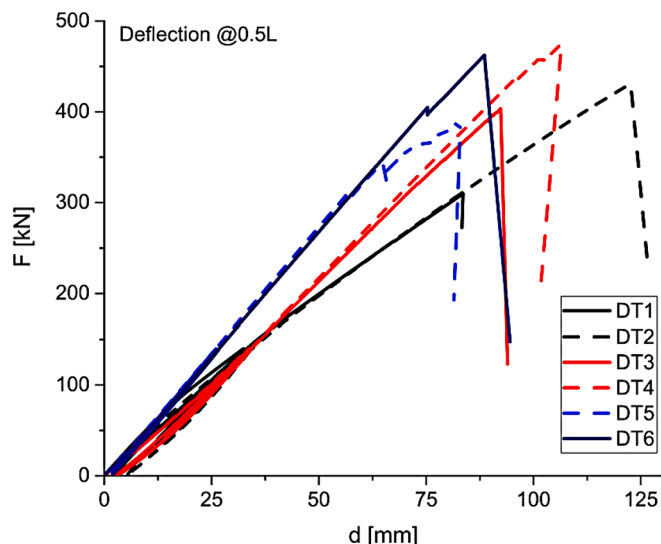


Fig. 14. Load-deflection curves at mid-span from full-scale bending tests.

Table 5

Results from destructive 4-point bending tests.

Test ID	F_{\max} [kN]	EI_{app} [kNm ²]	$d_{m,F_{\max}}$ [mm]	$S_{e,F_{\max}}$ [mm]	$S_{a,F_{\max}}$ [mm]
DT-1	310	47,693	84	3.4	2.0
DT-2	431	45,257	123	6.4	4.0
Avg. Type A	371	46,475	103	4.9	3.0
DT-3	403	56,213	92	1.5	1.3
DT-4	473	57,149	102	2.7	1.8
Avg. Type B	438	56,681	97	2.1	1.5
DT-5	391	60,598	83	0.2	0.2
DT-6	462	67,199	95	0.2	0.2
Avg. Type C	427	63,899	89	0.2	0.2

composite floor specimens. In all cases, failure was brittle, and occurred in the tension zone at a location close to mid-span of one of the two Glulam beams. In DT1, the flexural failure was observed on the right glulam, whereas, DT2 failed due to failure on the left glulam. Additionally, as seen in Fig. 16a, the finger joint on the right glulam in DT1 suddenly snapped and initiated failure at mid-span much earlier than DT2, e.g., DT1 failed at 28% lower loads compared to DT2. Since one of the beams appeared to be weaker than the other and commenced failure to the floors, there was an unequal amount of mid-span deflection observed. Fig. 16b illustrates that the 100×200 mm screws taken out after the tests were essentially undamaged due to the small relative slips at failure. In both Type B composite floors, when the 80×300 mm screws were taken out after the tests, these were similarly undamaged due to the small relative slips at failure, see Fig. 16d. Both Type C composite floors (DT5 and DT6) failed in a similar manner of brittle tension failure at the mid-span in one of the glulam beams (Fig. 16e). In DT6, CLT rolling shear failure was observed at the left CLT-glulam interface (Fig. 16f), potentially caused by stress concentrations along the edge.

3.5. Comparison between test results and predictions based on gamma method

The performance the tested composite floor systems was estimated based on the γ -method using the stiffness values recorded from small-scale tests, as summarized in Table 2. The resulting γ values for ultimate (γ_u) and serviceability (γ_{ser}) limit states for the floors with Type A, B, and C connectors are presented in Table 6. Based on these gamma values, the expected effective composite stiffness, EI_{cal} and the expected load-carrying capacity, F_{cal} , for each connector system were computed and compared against the experimentally obtained load-carrying capacity, F_{\max} , and the apparent bending stiffness, EI_{app} , respectively.

The experimental load-carrying capacities were roughly twice the estimated capacities, with the ratios F_{\max}/F_{cal} ranging from 1.9 to 2.3 for all three connector types, where F_{cal} is estimated with $\phi = 1.0$ and short-term duration loading of $K_D = 1.15$. This range is to be expected since F_{cal} was computed based on equations 3–8 with the material properties (listed in Table 1, and taken from CSA O86 [17]) are based on 5th percentile specified strength values as per ANSI PRG 320 [37] and CSA O122 [38]. The experimental stiffness of the system were very closely matched to the estimated stiffness, with the ratio of $EI_{\text{app}}/EI_{\text{cal}}$ ranging from 1.0 to 1.1 for all three connector types.

4. Conclusions

This paper presents experimental research on composite CLT glulam floors. The composite action was achieved using three connector options: Type A – partially-threaded STS installed at 90°; Type B – fully-threaded STS installed at 45°; and Type C – STS installed at 90° combined with an adhesive bond. The connector stiffness and strength were determined with small-scale shear tests. Vibration and quasi-static monotonic four-point bending tests were conducted on six full-scale

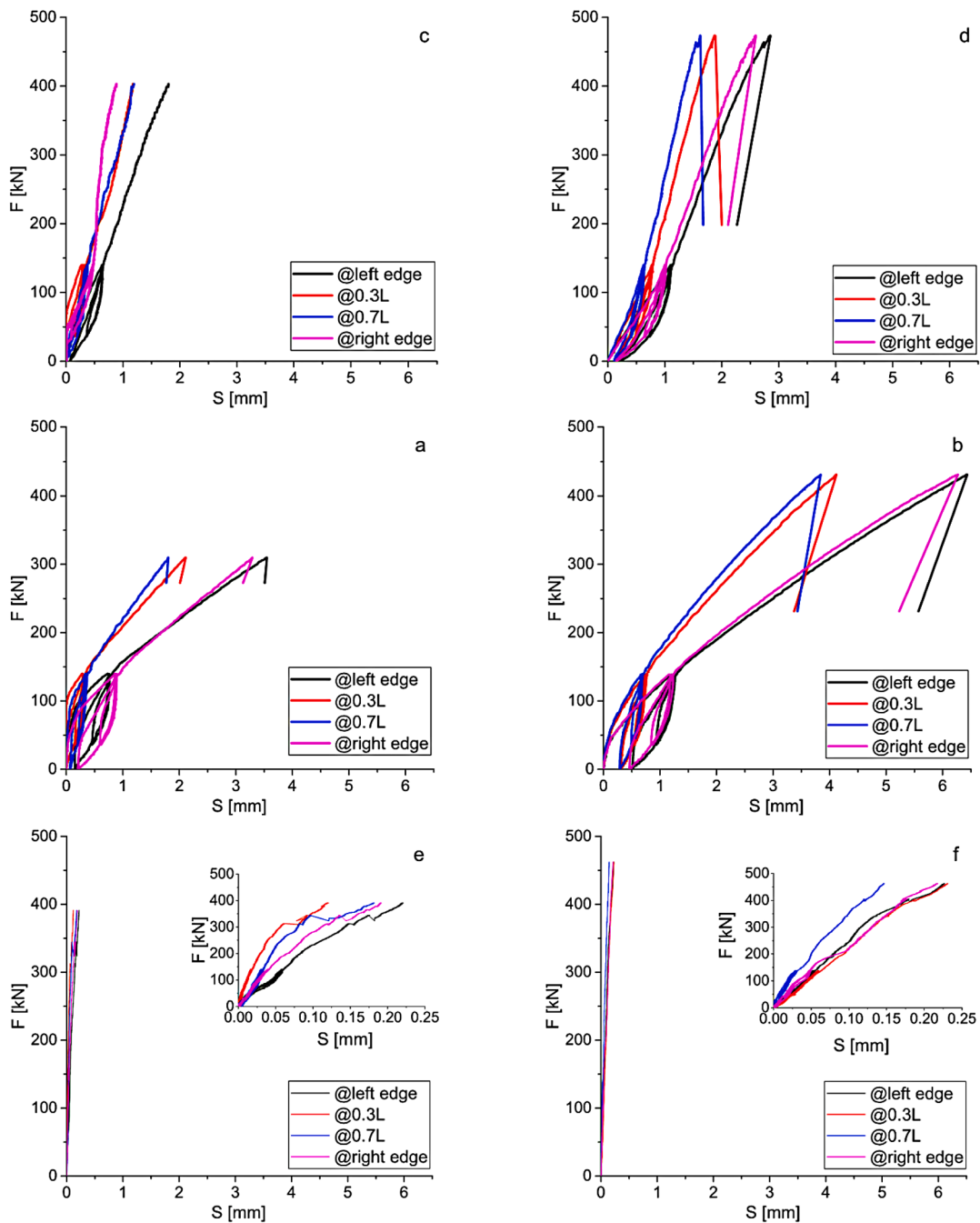


Fig. 15. TTC load-slip curves for: (a) DT1, (b) DT2, (c) DT3, (d) DT4, (e) DT5, and (f) DT6.

double T-beam floor segments consisting of 3-ply CLT panels and two glulam beams. The following conclusion can be drawn from this research:

Vibration tests were conducted on floor assemblies according to ISO 10137 and ISO 18324 to determine the floors' natural frequencies and acceleration responses. The fundamental natural frequencies of all specimens were between 12 and 13 Hz, with no significant differences among the three groups. The damping ratio of the fundamental frequency mode was around 2.4% on average. The limited variation demonstrates a consistent initial stiffness of the system, regardless of connector type, for low amplitude loads.

A reduction in span increased the fundamental natural frequency, and thus led to acceptable vibration controlled span around 7.2 m with a fundamental natural frequency of 17.5 Hz, which was confirmed by subjective evaluations standing observers with one walking person.

The load-deformation behaviour observed in the full-scale testing was linear up to failure. Although there were significant differences between the load-carrying capacities within each group of composite systems, the differences in stiffness between the two replicates from each group were very minor.

The connectors were designed with sufficient shear strength and the failure mechanism in all specimens was observed brittle tension failure at mid-span initiated at either one of the two glulam beams. All floors exhibited similar load-carrying capacity.

The bending stiffness of floors (EI) was a function of their gamma values. The ratio between experimental and expected was close to 1.0 for all three connector types, demonstrating the adequacy of applying the gamma method to predict the bending stiffness of composite floors. The experimentally obtained load-carrying capacity exceeded the estimated values by roughly a factor of 2.0, providing an acceptable level of

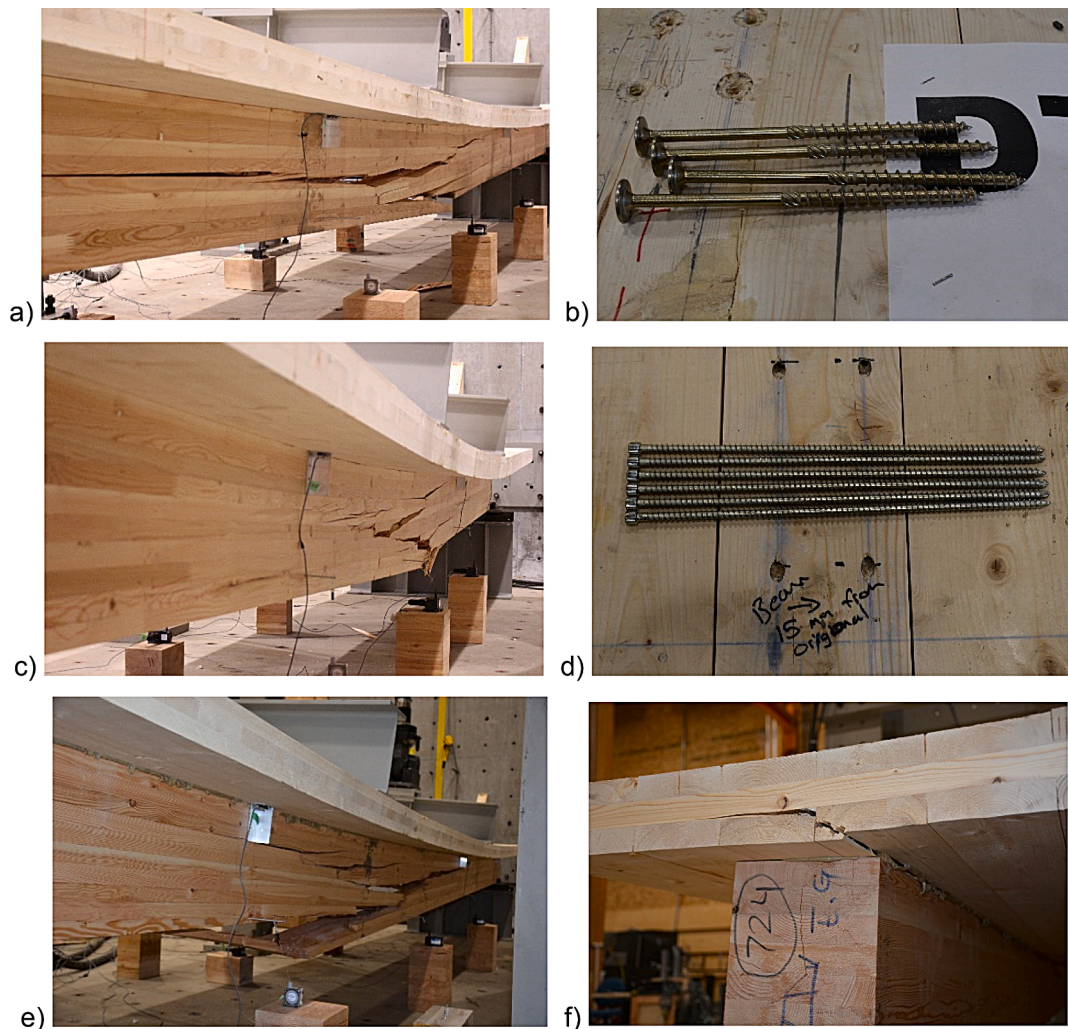


Fig. 16. Failed specimen: (a) flexural failure of one glulam beam Type A, (b) screws taken out from failed floor Type A; (c) flexural failure of one glulam beam Type B, (d) screws taken out from failed floor Type B; (e) flexural failure of one glulam beam Type C, (f) CLT rolling shear failure Type C.

Table 6
Comparison of test results versus predictions.

Connector	γ_{ser} [-]	γ_u [-]	EI_{cal} [kNm ²]	F_{cal} [kN]	F_{max} / F_{cal} [-]	EI_{app} / EI_{cal} [-]
Type A	0.36	0.18	41,190	168	2.2	1.1
Type B	0.68	0.69	52,277	193	2.3	1.1
Type C	0.99	0.99	62,151	230	1.9	1.0

safety.

The findings from this research supported the design and construction of CLT-glulam composite floors for two new school buildings. Although the vibration tests did not meet the required performance criteria, the actual floor boundary conditions are expected to lead to satisfactory performance. In-situ testing will evaluate the vibration performance of the floors.

Data availability

The raw/processed data required to reproduce these findings cannot be shared at this time as the data also forms part of an ongoing study. Some or all data, models, or code that support the findings of this study are available from the corresponding author upon reasonable request.

CRedit authorship contribution statement

Md Shahnewaz: Conceptualization, Methodology, Investigation,

Formal analysis, Visualization, Writing – original draft. **Carla Dickof:** Conceptualization, Methodology, Investigation. **Jianhui Zhou:** Investigation, Formal analysis, Visualization, Writing – original draft. **Thomas Tannert:** Conceptualization, Methodology, Investigation, Supervision, Writing – review & editing.

Declaration of Competing Interest

The authors declare that they have no known competing financial interests or personal relationships that could have appeared to influence the work reported in this paper.

Acknowledgements

The project was supported by Natural Resources Canada (NRCAN) through the Green Construction through Wood (GCWood) Program. The support by the UNBC technicians Michael Billups and Ryan Stern and undergraduate research assistants Anthony Bilodeau and Jaqulyn Alexandre is greatly appreciated.

References

[1] Green M, Karsh E. The case for tall wood buildings. Vancouver: Wood Enterprise Coalition; 2012.
 [2] Tannert T, Follesa M, Fragiaco M, Gonzalez P, Isoda H, Moroder D, et al. Seismic design of cross-laminated timber buildings. Wood Fiber Sci 2018;3–26.

- [3] Brandner R, Flatscher G, Ringhofer A, Schickhofer G, Thiel A. Cross laminated timber (CLT): overview and development. *Eur J Wood Wood Prod* 2016;74(3): 331–51.
- [4] Gagnon S, Pirvu C. *Cross Laminated Timber (CLT) Handbook*. Vancouver, BC, Canada: FPInnovations; 2020.
- [5] Dietsch P, Brandner R. Self-tapping screws and threaded rods as reinforcement for structural timber elements—A state-of-the-art report. *Constr Build Mater* 2015;97: 78–89.
- [6] Hossain A, Danzig I, Tannert T. Cross-laminated timber shear connections with double-angled self-tapping screw assemblies. *J Struct Eng* 2016;142(11): 04016099.
- [7] Zhang X, Popovski M, Tannert T. High-capacity hold-down for mass-timber buildings. *Constr Build Mater* 2018;164:688–703.
- [8] Dias AMPG, Skinner J, Crews K, Tannert T. Timber-concrete-composites increasing the use of timber in construction. *Eur J Wood Wood Prod* 2016;74(3):443–51.
- [9] NBCC. National building code of Canada, Canadian commission on building and fire codes. Ottawa, ON: National Research Council of Canada; 2020.
- [10] IBC. The international building code (IBC). Country Club Hills, IL, USA: International Code Council; 2021.
- [11] Shahnewaz M, Popovski M, Tannert T. Resistance of cross laminated timber shear walls for platform-type construction. *J Struct Eng, ASCE*, 2019;145(12):04019149.
- [12] Shahnewaz M, Popovski M, Tannert T. Deflection of cross laminated timber shear walls for platform-type construction. *Eng Struct* 2020;221(2020):111091.
- [13] Vancouver school board (VSB). <https://www.vsb.bc.ca> [Accessed September 2020].
- [14] Natural Resources Canada (NRCAN). Green Construction through Wood (GCWood) Program. <https://www.nrcan.gc.ca> [Accessed September 2020].
- [15] Smith I. Vibrations of timber floors: serviceability aspects. In: Thelandersson S, Larsen HJ, editors. *Timber engineering*. Wiley; 2003. p. 241–66.
- [16] Weckendorf J, Toratti T, Smith I, Tannert T. Vibration serviceability performance of timber floors. *Eur J Wood Wood Prod* 2016;74(3):353–67.
- [17] CSA O86-19, Engineering Design in Wood. Canadian Standard Association, Ottawa, Ont; 2019.
- [18] Murray TM, Allen DE, Ungar EE, Davis DB. Vibrations of steel-framed structural systems due to human activity: AISC design guide 11; 2016.
- [19] Smith AL, Hicks SJ, Devine PJ. SCI P354: Design of floors for vibration: a new approach. Ascot: The Steel Construction Institute; 2009.
- [20] Fanella DA, Mota M. Design guide for vibrations of reinforced concrete floor systems. Concrete Reinforcing Steel Institute (CRSI): Schaumburg, IL, USA; 2014.
- [21] Breneman. US mass timber floor vibration design guide. Woodworks. <https://www.woodworks.org> (accessed February 8, 2021); 2020.
- [22] Yeoh D, Fragiaco M, De Franceschi M, Heng BK. State of the art on timber-concrete composite structures: Literature review. *J Struct Eng* 2011;137(10): 1085–95.
- [23] Shahnewaz M, Jackson R, Tannert T. CLT concrete composite floors with steel kerf plate connectors. *Construct Build Mater* 2022;319:126092. <https://doi.org/10.1016/j.conbuildmat.2021.126092>.
- [24] Tannert T, Endacott B, Brunner M, Vallée T. Long-term performance of adhesively bonded timber-concrete composites. *Int J Adhes Adhes* 2017;72:51–61.
- [25] Tannert T, Gerber A, Vallee T. Hybrid adhesively bonded timber-concrete-composite floors. *Int J Adhes Adhes* 2019;97:102490.
- [26] O’Loinsigh C, Oudjene M, Ait-Aider H, Fanning P, Pizzi A, Shotton E, et al. Experimental study of timber-to-timber composite beam using welded-through wood dowels. *Constr Build Mater* 2012;36:245–50.
- [27] Giongo I, Piazza M, Tomasi R. Out of plane refurbishment techniques of existing timber floors by means of timber to timber composite structures. World Conference in Timber Engineering, July 15-19, 2012, New Zealand; 2012.
- [28] Jacquier N, Girhammar UA. Tests on glulam-CLT shear connections with double-sided punched metal plate fasteners and inclined screws. *Constr Build Mater* 2014; 72:444–57.
- [29] Masoudnia R, Hashemi A, Quenneville P. Predicting the effective flange width of a CLT slab in timber composite beams. *J Struct Eng* 2018;144(7):04018084.
- [30] Giongo I, Schiro G, Walsh K, Riccadonna D. Experimental testing of pre-stressed timber-to-timber composite (TTC) floors. *Eng Struct*, 2019; 109808.
- [31] Bedon C, Fragiaco M. Numerical analysis of timber-to-timber joints and composite beams with inclined self-tapping screws. *Compos Struct* 2019;207: 13–28.
- [32] Riccadonna D, Walsh K, Schiro G, Piazza M, Giongo I. Testing of long-term behaviour of pre-stressed timber-to-timber composite (TTC) floors. *Constr Build Mater* 2020;236. 117596.
- [33] ETA-20/0893. Prefabricated wood-based loadbearing stressed skin panels. European Technical Approval, ETA-20/0893, Denmark; 2020.
- [34] Schober KU, Tannert T. Hybrid connections for timber structures. *Eur J Wood Wood Prod* 2016;74(3):369–77.
- [35] CEN. EN 1995-1-1: Eurocode 5: design of timber structures—part 1-1: general—common rules and rules for buildings. Brussels, Belgium: European Committee for Standardization; 2004.
- [36] Möhler K. Über das Tragverhalten von Biegeträgern und Druckstäben mit zusammengesetzten Querschnitten und nachgiebigen Verbindungsmitteln (Doctoral dissertation); 1956.
- [37] ANSI/APA PRG 320. “Standard for performance-rated cross-laminated timber.” American National Standards Institute. New York, NY, USA; 2017.
- [38] CSA O122. Structural glued-laminated timber. Canadian Standards Association, Rexdale, Ontario, Canada; 2016.
- [39] LePage Technical Data Sheet, LePage PL Premium Max Construction Adhesive. <https://dm.henkel-dam.com> [Accessed December 2021].
- [40] ASTM D3498. Standard Specification for Adhesives for Field-Gluing Plywood to Lumber Framing for Floor Systems. West Conshohocken: ASTM International; 2017.
- [41] CCMC. Evaluation Report CCMC 13677-R, SWG ASSY® VG Plus and SWG ASSY® 3.0 Self-Tapping Wood Screws; 2018.
- [42] Solutions MTC. Structural screw design guide. BC, Canada: Surrey; 2020.
- [43] ETA-11/0190.. Self-tapping screws for use in timber constructions. European Technical Approval 2018;ETA-11/0190.
- [44] EN 408. Timber structures—Structural timber and glued laminated timber—Determination of some physical and mechanical properties. Brussels, Belgium: European Committee for Standardization; 2010.
- [45] EN 26891: 1991. Timber structures—Joints made with mechanical fasteners—General principles for the determination of strength and deformation characteristics. Brussels, Belgium: European Committee for Standardization; 2013.
- [46] ASTM E2126. Standard test methods for cyclic (reversed) load test for shear resistance of walls for buildings. West Conshohocken: ASTM International; 2011.
- [47] ISO. 10137: Bases for design of structures-serviceability of buildings and walkways against vibrations. International Standard Organisation 2007.
- [48] ISO. 18324: Timber structures –Test methods- Floor vibration performance. International Standard Organisation 2016.
- [49] ISO. 2631-2: Mechanical vibration and shock—Evaluation of human exposure to whole-body vibration—Part 2: Vibration in buildings (1 Hz to 80 Hz). International Standard Organisation 2003.
- [50] ISO. TR 21136: Timber structures – Vibration performance criteria for timber floors. International Standard Organisation 2017.